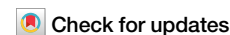



<https://doi.org/10.1038/s44455-025-00006-5>

Fast hybrid multiple scattering theory for full-wave simulation of metasurface with substrate

Leung Tsang , Zhenming Huang & Jongwoo Jeong

It is important to characterize accurately the metasurface device for the desired performance using solutions of Maxwell equations for 3D problems. In this paper, we perform a full-wave simulation of metasurfaces with thousands of scatterers above a dielectric substrate, which has not been done previously. To account for the substrate, we developed a new version of the Fast Hybrid Multiple Scattering Theory Method (FHMSTM) by combining Vector Plane Waves (VPW) and Vector Spherical waves (VSW). Transformations between VPW and VSW are used in Foldy–Lax multiple scattering equations. The results are illustrated for two examples: (i) Orbital Angular Momentum (OAM) metasurfaces and (ii) metamirror metasurfaces. We illustrate the case of 5024 silicon elliptical nanopillar scatterers above a dielectric substrate. The CPU and memory requirements are, respectively 1023.2 s and 100 Mb on a standard personal computer. This simulation was previously very difficult for commercial software.

There has been rapid growth in the science and technology of metasurfaces in optics, microwaves, and terahertz frequencies. In optics, metasurfaces are an important part of metaoptics and have been used to focus light, form efficient diffractive elements, and control the polarization of light^{1–3}. In the microwave domain, metasurfaces enable new platforms for communications, antennas, radars, and remote sensing⁴. With the advances of 3D printing technologies, metasurfaces can be fabricated for terahertz devices, bridging the gap between photonics and microwaves for next-generation communications and imaging^{5,6}. Metasurfaces have also been applied to quantum optics for the control of non-classical light⁷. In ref. 8, metasurfaces are utilized to increase quantum entanglement between two qubits that are far apart by increasing their coherent interactions. There has been a huge growth of publications in metasurfaces in recent years⁹. Theoretical investigations of electromagnetic fields of metasurfaces have been conducted by analytical and numerical methods. Metasurfaces have many unit cells, with each cell containing a scatterer of complicated shape, making the problem formidable. Analytical methods, based on quasi-static approximation, represent unit cells in metasurfaces by circuit elements¹⁰. However, circuit models neglect the radiation properties of the scatterers and the wave interactions among unit cells. Quasi-analytical methods have also been used with restrictive assumptions¹¹. In the metasurface design process, it is important to use full-wave simulations of Maxwell equations for 3D problems to accurately characterize the wave scattering of the metasurface for the desired performance. In Computational Electromagnetic Methods (CEM), spatial discretization is used. CEM methods include the finite

element method (FEM)¹², the finite difference method, which can be in either time domain (FDTD)¹³ or frequency domain (FDFD)¹⁴, and the method of moments (MoM), which has been accelerated by the Multilevel Fast Multipole Method (MLFMM)¹⁵. Besides, many specialized methods have been developed^{16–19}. The Commercial software HFSS and COMSOL employ the FEM, the commercial software CST uses FIT (finite integration technique, which is similar to FDTD), and the commercial software FEKO uses MoM with Multilevel Fast Multipole (MLFMM). The full-wave simulations of metasurfaces have been computed by using COMSOL and CST^{20–22}. However, the full-wave simulations in commercial software require large CPU time and memory. In ref. 23, 3 × 10⁵ simulation datasets using the finite element method (FEM) were computed to provide machine learning training for optimal design of metasurfaces. The training data collection procedure using FEM requires High-Performance parallel computing. Recently, artificial intelligence and machine learning have been adopted in the design of metasurfaces^{9,24}. The forward prediction algorithms of simulations are time-consuming and hard to realize an ideal meta-atom spectrum²⁵. The machine learning method is an alternative, but it still requires time-consuming training process using expensive GPU clusters. It is also difficult to use commercial software to compute electrically large 3D targets of complicated structures (>10 wavelengths) at a reasonable memory cost. On the other hand, optical metasurfaces are fabricated with a large number of unit cells.

A highly efficient simulation method, Fast Hybrid Multiple Scattering Theory Method (FHMSTM), is developed in this paper for the case of a

Department of Electrical Engineering and Computer Science, University of Michigan, Ann Arbor, MI, USA.  e-mail: leutsang@umich.edu

metasurface with scatterers above a dielectric substrate (which can be extended in the future to a half-space/single/multi-layer substrate, PEC, or even a rough surface or a grating). Various substrates can be represented by deriving the T matrix of substrates consisting of multiple layers. It is shown that, because of high computational efficiency, the case of thousands of scatterers above a dielectric substrate can be computed on a personal computer. The computational efficiency achieved in this paper will significantly boost the design and optimization of the metasurfaces. Previously, we developed the Fast Hybrid Multiple Scattering Method for full-wave simulations of multiple scattering in vegetation and forests for applications in satellite microwave remote sensing of soil moisture, agriculture fields, and forests^{26,27}. In this previous version, the plants and trees are in an infinite medium without a substrate below them. In a separate paper²⁸, we apply the FHMSTM to metasurfaces consisting of scatterers in an unbounded medium, also without a substrate.

In a metasurface, often the scatterers are placed above a dielectric substrate (Fig. 1). Thus, it is important to include the dielectric substrate in full-wave simulations. To account for the presence of the substrate below the metasurface scatterers, we developed, in this paper, a new version of the Fast Hybrid Multiple Scattering Theory Method (FHMSTM) by combining Vector Plane Waves (VPW) and Vector Spherical waves (VSW). In Fig. 1, we show the geometrical configuration of a laser beam incident on the metasurface with unit cells placed above the dielectric substrate. The extent of the laser beam is confined within the domain of the unit cells of the metasurface (Fig. 1). Thus, in the full-wave simulations of FHMSTM in this paper, we treat the dielectric substrate as infinite in extent. The dielectric substrate is treated as a single scatterer, and the T matrix of the substrate is cast in Vector Plane Waves (VPW).

In the T matrix of VPW, the evanescent waves of the dielectric substrate are included by using complex angles. We use the T matrix of Vector Spherical waves (VSW) for the scatterers. Foldy–Lax multiple scattering equations are formulated in terms of Vector Spherical waves (VSW) and Vector Plane waves (VPW). Transformations between VPW and VSW are applied that include evanescent waves and near fields. In the Foldy–Lax formulation of multiple scattering, T matrices are used, and spatial discretizations are not used. Numerical solutions of the Foldy–Lax equations are accelerated by using FFT. To validate the accuracy of FHMSTM, we first study the case of spheres (details can be found in the supplementary document) and cubes above the dielectric substrate and make comparisons with results from commercial software. The FHMSTM are next illustrated with two examples of metasurfaces that have found applications in metaoptics: (i) Orbital Angular Momentum (OAM) metasurfaces^{29,30} and (ii) Metamirror³¹. For the OAM case, we consider 5024 silicon elliptical nanopillar scatterers above a dielectric substrate. The CPU and memory

requirements for FHMSTM are, respectively, 1023.2 s and 100 Mb on a standard laptop. By comparing CPU and memory requirements, the FHM method is shown to be more efficient than commercial software by three orders of magnitude for CPU time and four orders of magnitude for memory. This simulation was previously very difficult for commercial software.

Results

In this section, we first compare the results for a large number of scatterers with FEKO, a commercial CEM software, to demonstrate the large-scale computational capability of the proposed method. Then, two metasurface cases are presented. The validation of accuracy is provided in the supplementary document.

Large number of scatterers of cubic shapes

We give an example to serve as proof of large-scale computation ability. We compare the results of large numbers of scatterers with FEKO. Here, we are using cubic scatterers with a dimension of $0.12\lambda \times 0.12\lambda \times 0.12\lambda$ (Fig. 2). The grid distance is 0.24λ , and the lowest scatterer touches the flat plane. A $N_{\max} = 2$ is used. All calculations are carried out on an 8-core common computer with 32 GB of memory. Since FEKO does not allow a surface touch to the dielectric plane, we give a small offset of 0.001λ . Here we use the fine-mesh option of FEKO. The results of 1024 scatterers with horizontal wave incidence are shown in Fig. 4. Figure 3 compares the CPU times between FEKO and FHMSTM. Table 1 is a list of memory requirements. The memory consumption of FHMSTM is almost linear when the number of scatterers is large and is less than 100 MB for 4096 scatterers, which is significantly less than FEKO. The CPU requirement of Fig. 3 and the

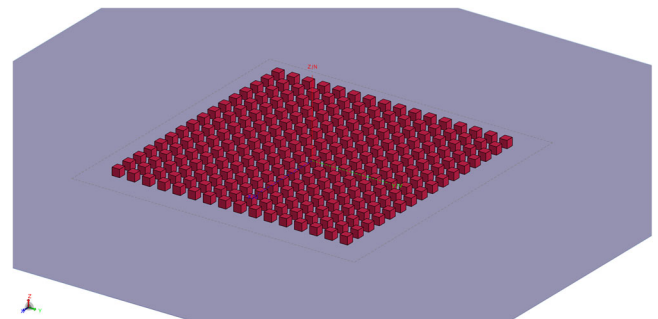


Fig. 2 | 1024 cubic scatterers.

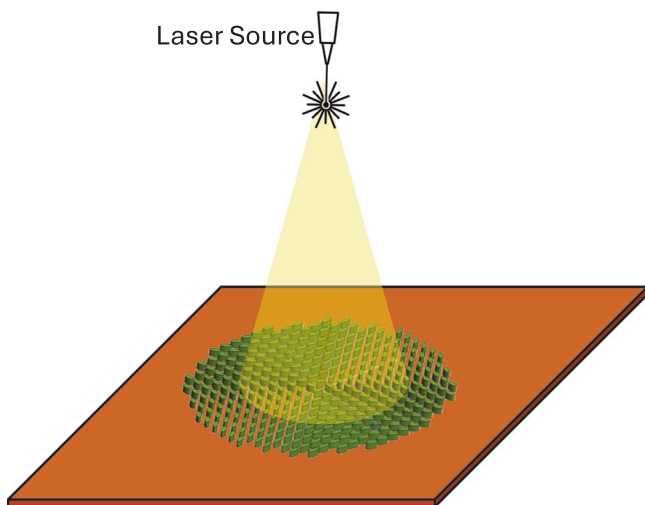


Fig. 1 | A laser beam incident on the metasurface.

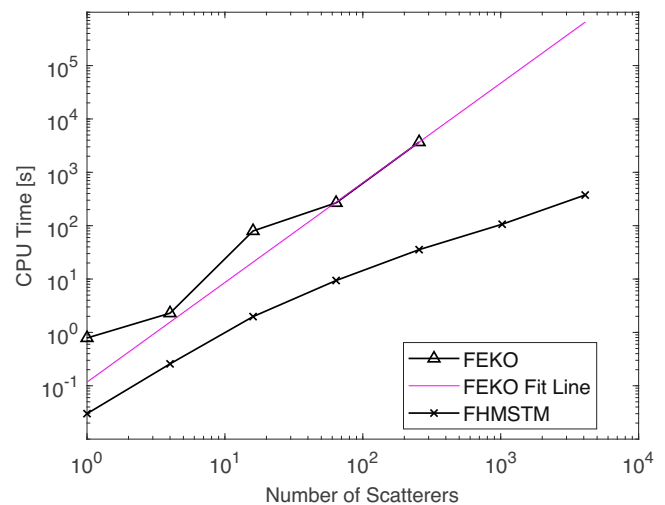


Fig. 3 | Speed of FHMSTM and FEKO (fine mesh).

Table 1 | Memory consumption of FEKO (fine mesh) and FHMSTM

Scatterers number	1	4	16	64	256	1024	4096
FEKO, fine mesh	27.0 MB	27.3 MB	46.8 MB	662.0 MB	10.2 GB	159.6 GB ^a	2506 GB ^a
FHMSTM	16 KB	16 KB	16 KB	1.0 MB	4.0 MB	16.0 MB	64.1 MB

^aAnticipate results.

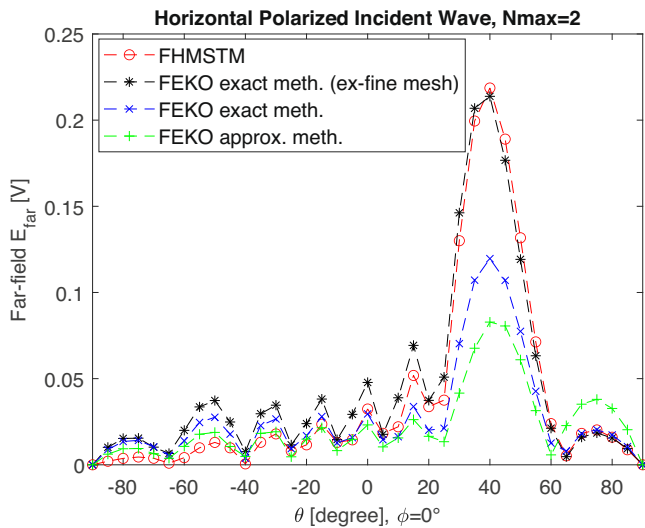


Fig. 4 | Far-field scattering amplitude of 256 cubic scatterers with horizontal polarized incidence. Comparisons of the FHMSTM with the results of the three options of FEKO (i) approximate reflection coefficient, (ii) exact with fine-mesh, and (iii) exact with extra-fine mesh.

memory requirement of Table 1 show that we cannot run FEKO for 1024 scatterers nor 4096 scatterers.

For 256 scatterers, it requires an FEKO CPU of 3683 s compared with 35 s using FHMSTM. The FHMSTM is 104 times faster than FEKO for 256 scatterers. The memory requirement for 256 scatterers for FHMSTM is 4.0 MB, which is 2611.2 times less than the 10.2 GB required for FEKO.

For 4096 scatterers, FEKO is anticipated to use 652,921 s and 2506 GB, which are 1740 and 40,016 times greater than FHMSTM. The anticipations are based on a $Y(N) = aN^b$ model, and the values of b are slightly smaller than 2.

It indicates that it is difficult to use FEKO to solve the case of thousands of scatterers without extensive high-performance computing resources. All of the tests are carried out on an 8-core common computer with 32 GB of memory.

In Fig. 4, we compare the results of the far-field scattering amplitudes as a function of scattered angles of 256 cubic scatterers with horizontally polarized incidence. Four results are shown: the result of FHMSTM and the results of the three options of FEKO (i) approximate reflection coefficient, (ii) exact with fine-mesh, and (iii) exact with extra-fine mesh. The results of the three options of FEKO do not agree with each other. The FEKO results of fine mesh and reflection coefficient approximation are inaccurate. Assuming that FEKO extra-fine mesh is more accurate, the FHMSTM results are validated as the results show good agreement with FEKO of the extra-fine-mesh option, in particular in the angle region around the main peak.

Next, we illustrate the proposed FHMST to two applications of metasurfaces with a dielectric substrate to demonstrate the computation efficiency of FHMSTM.

Metasurfaces consisting of different scatterers

OAM metasurfaces are used to manipulate light to produce vortex beams with orbital angular momentum (OAM)^{29,32}.

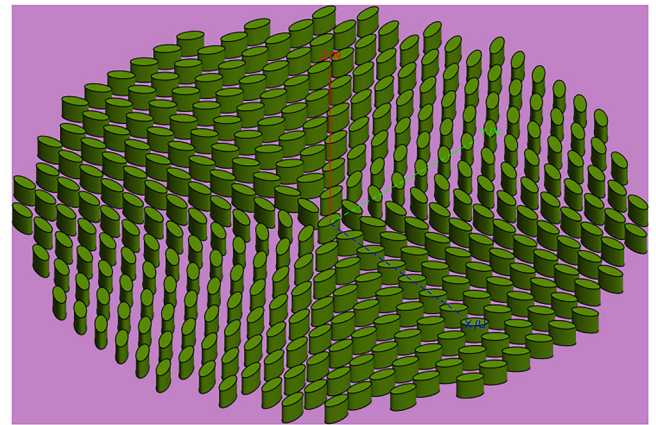


Fig. 5 | Illustration of an OAM reflection metasurface.

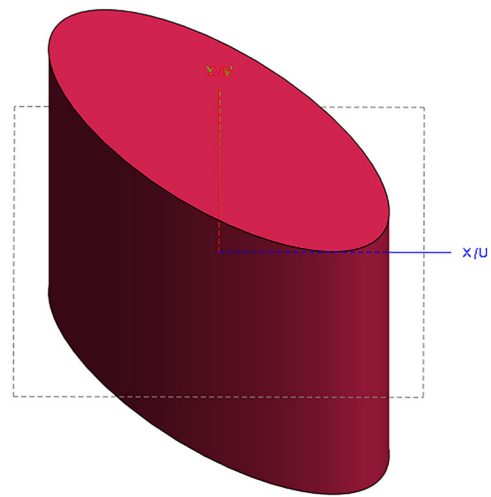


Fig. 6 | Unit cell.

The metasurface²⁹ in Fig. 5 has been used to generate reflected Orbital angular momentum (OAM) waves from an LCP/RCP incident wave.

The radius of this metasurface is set as 20.64λ , and the number of scatterers is 5024. If the working wavelength is set as 1550 nm, the radius of the etching area will be $32\ \mu\text{m}$. The scatterers lie on a dielectric substrate as illustrated.

Figure 6 shows the scattering structure of a single unit cell of a silicon elliptical nanopillar, which performs as a resonator. The different scatterers in Fig. 5 of the OAM metasurface are obtained by rotating the Euler angle α according to a helical phase term. So, scatterers in each unit cell are different from the point of view of the incident wave. The ground plane is made of a fused silica substrate. For this simulation case, the topological charge l is chosen as -2 , and the incident wave is RCP with an incident angle of 0° .

Using the proposed FHMSTM, we perform full-wave simulations and obtain the far-field scattering pattern. The results are shown in Fig. 7, which shows the OAM cone-like far field. The calculation time of FHMSTM is

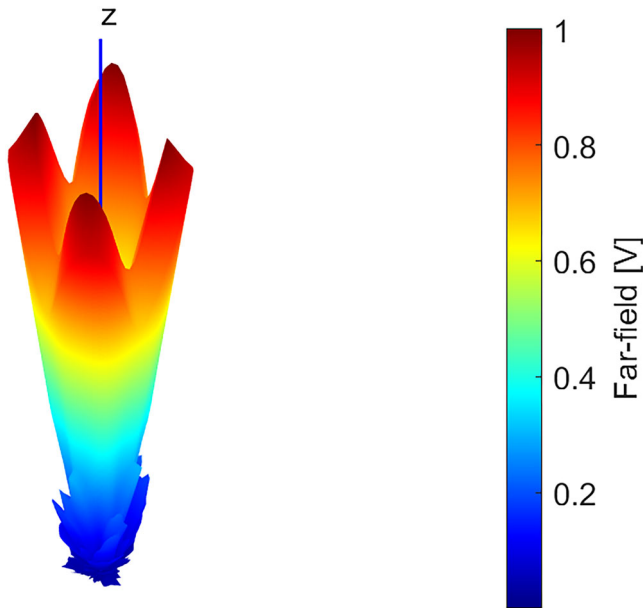


Fig. 7 | Far-field of the meta-surface with an RCP incident wave.

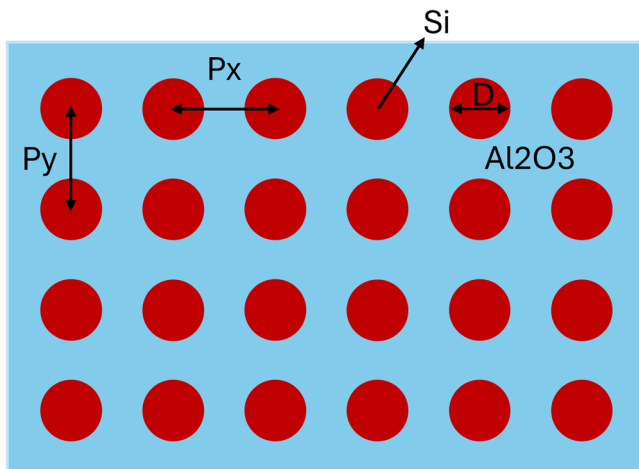


Fig. 8 | A metamirror.

1023.2 s, and the memory requirement is 100.2031 MB. We could not apply FEKO to solve this case as FEKO requires more memory than the 192 GB of our server.

Wavelength-selective metamirror

The metasurface (Metamirror)³¹ of Fig. 8 is designed to operate at a target of $\lambda_1 = 1064$ nm, consisting of cylindrical Si unit cells on an Al₂O₃ substrate. The Px and Py are chosen as 416 nm. The height and diameter of the cylinders are 211 and 297 nm, respectively.

In this case, we simulate 6400 (80 × 80) unit cells. The area of this metasurface is 1107.5584 μm^2 . The reflection efficiency is calculated through

$$\eta_r = \frac{P_{ref}}{P_{in}}$$

where P_{ref} is the reflected energy toward the z-direction calculated within a surface that has the same area as the metasurface and 20λ above it. The P_{in} is the energy of the plane wave incident on the surface of $788.2425 \mu\text{m}^2$ with an incident angle of 0° .

Figure 9 shows the near field. The proposed FHMSTM requires 3818 s to finish the test case. The computed reflection efficiency is 90.85%. This case

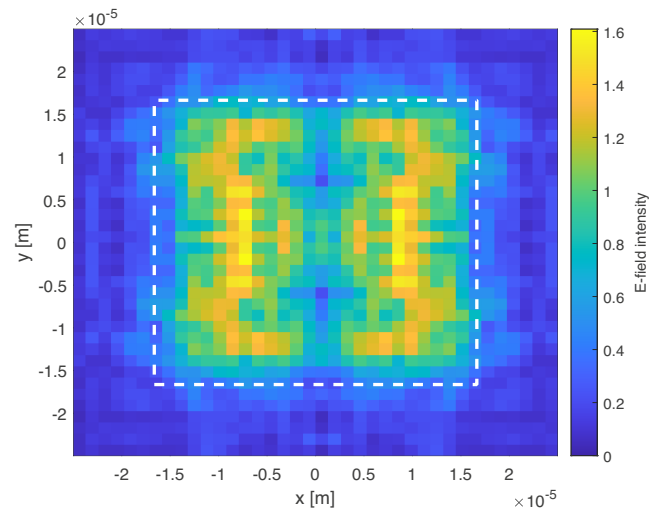


Fig. 9 | Scattered field of the metamirror at $z = 20 \lambda$. The white dashed line is the area of the metamirror and the region of calculating the reflection coefficient.

is slower than the OAM metasurface because a significant amount of time is spent calculating the near field. Although not yet implemented, this part can be parallelized to further improve efficiency.

In addition to computational efficiency, another advantage of the results of FHMSTM is that the edge effects are shown clearly.

Discussion

Among the numerical software, only FEKO can be used to calculate problems with infinite substrates. For simulations of a metasurface with a substrate, the laser beam is confined to within the metasurface so that the assumption of the infinite substrate is appropriate. Also, the use of infinite substrates will eliminate edge effects. Therefore, FEKO is used for baseline comparisons.

In comparison with the demonstrations of the scatterers and metasurface simulation based on commercial software (FEKO), the proposed method is 104 times faster than FEKO fine-option for 256 scatterers. We show by projection that it is 1,740 times faster for 4096 scatterers. In memory requirement for 256 scatterers, FHMSTM requires 2611.2 times more memory than FEKO fine-mesh option and 40,016 times less by projection for 4096 scatterers. The first reason why the FHM is so fast is that a single scatterer is characterized as a whole, which only has tens of unknowns on the basis of VSW, and no air regions need to be solved. FEKO requires space discretization of the scatterers of complicated shapes, and all the space discretizations are coupled in a problem of thousands of scatterers. For FEM methods such as HFSS, the situation is even worse than FEKO because the air region between the scatterers needs to be spatially discretized. Absorbing boundary conditions need to be set up for FEM that further increase the region of spatial discretization. The second reason is that the T matrix of a single scatterer is obtained. The T matrix is stored in a library and is reusable for all problems. Also, when the scatterers are rotated, which is often the case in metasurface fabrication, the T matrix is rotated without recalculation. The third reason is that for the Foldy–Lax multiple scattering equations of many scatterers, including the substrate, there is no spatial discretization in the Foldy–Lax equations. The T matrices of VSW and VPW are utilized. The fourth reason is that the Foldy–Lax equations are solved by FFT even though the scatterers are different.

FEKO faces convergence challenges, which often require an extremely fine mesh for multi-scattering problems and, in some cases, may fail to converge entirely. As shown in Fig. 4, we also observe that the results of the approximation method (FEKO) are significantly lower than the exact method (FEKO) around the main peak. It further demonstrates that FEKO is not robust for multi-scattering problems with a substrate. We believe our proposed FHMSTM method should provide good accuracy because the

formulation of multiple scattering and the numerical implementations are rigorous.

In this paper, we develop a new version of FHMSTM for full-wave simulations of metasurfaces consisting of thousands of unit cells above a dielectric substrate. We treat scattering by metasurfaces as a problem in multiple scattering of waves, assuming that the scattering by a single scatterer is completely known from the “single scatterer solution”. The new version of FHMSTM presented in this paper have the formulations that (i) two vector wave expansions are used, the dielectric substrate with the T matrix of the substrate represented by Vector Plane waves and the T matrix of the scatterer are in terms of Vector Spherical waves (ii) the Foldy–Lax equations of the wave interactions between scatterers in VSW and the dielectric substrate in VPW including near fields and evanescent waves, and (iii) the transformations between VPW and VSW. In numerical implementations, the T matrix of the scatterer is computed only once, and if the scatterer is rotated, the T matrix is rotated without new calculations. Summations of scattered waves in Foldy–Lax equations are computed speedily by FFT. The accuracies of the FHMSTM method are validated by comparing it with that of commercial software for problems with a smaller number of unit cells. The results are illustrated for OAM metasurface and meta-mirrors with thousands of scatterers. The CPU and memory requirements of FHM are much more efficient by approximately three and four orders of magnitude than commercial software for 4096 scatterers. The FHMSTM allows design and full-wave simulations of metasurfaces tasks to be carried out on a personal computer, which is significantly less expensive than CPU/GPU clusters that are used in the traditional design and optimization process. Multiple scattering theory has been successfully applied to complicated structures such as 3D metamaterial structures^{33,34}. In addition, the Fast Hybrid Multiple Scattering Method can be applied to diverse applications of multiple scattering problems of many research communities, including remote sensing^{27,28}, signal integrity in microelectronics³⁵, photon transport in colloidal suspensions³⁶, radar scattering by icy satellites in planetary science³⁷, backscattering enhancement of photon pairs in quantum entanglement³⁸, wireless communications channel modeling³⁹, etc.

This paper opens the door for large metasurfaces with substrates and layers, and opens the door for many exciting new physical results that have been impossible to simulate. We are now extending the model to multi-layered substrates by using the T matrix of layered medium, which consists of reflection coefficients of plane waves and evanescent waves.

Methods

In a multiple scattering problem, the solution of a single scatterer is assumed to be known. That means for an arbitrary exciting field upon the single scatterer, the scattered fields and the internal fields of the single scatterer are calculated, such as by the CEM method of space discretizations. We shall label this as the “single scatterer solution”.

Since the “single scatterer solution” is known, the unknown in a multiple scattering problem is the final exciting field on the scatterer. The Foldy–Lax multiple scattering equations^{40,41} were rigorously derived from Maxwell equations^{42,43}. They are formulated in terms of the final exciting fields of all the scatterers^{43,44}.

Consider N scatterers above a surface. Let E^{inc} be the incident wave, T_p , $p = 1, 2, \dots, N$ be the T matrix of the scatterers, T_{sur} is the T matrix of the surface.

Then the multiple scattering equations of Foldy–Lax govern the final exciting field, E_q^{ex} , $q = 1, 2, \dots, N$ of the scatterers and E_{sur}^{ex} , the final exciting field of the surface. The FL equations, in symbolic form, are

$$E_q^{ex} = E^{inc} + \sum_{p=1, p \neq q}^N G_{qp} T_p E_p^{ex} + G_{q,sur} T_{sur} E_{sur}^{ex} \quad (1)$$

$$E_{sur}^{ex} = E^{inc} + \sum_{p=1}^N G_{sur,p} T_p E_p^{ex} \quad (2)$$

where G_{qp} is the propagator from scatterer p to scatterer q , $G_{q,sur}$ is the propagator from the surface to the q th scatterer, and $G_{sur,p}$ is the propagator from the p th scatterer to the surface.

The following are observations of the Fold–Lax multiple scattering equations:

1. The final exciting fields are the unknowns. The final exciting field of a scatterer is due to the incident wave plus the scattered fields from other scatterers to that scatterer. The advantage of the Foldy–Lax equations is that they only require scattering from a scatterer to all other scatterers. The dielectric substrate is a scatterer with T matrix T_{sur} . The Foldy–Lax equations do not require the field solutions everywhere.
2. The use of the T matrix is to calculate scattering to other scatterers. The T matrix only requires a subset of information from the “single scatterer” solution.
3. The scattering from one scatterer to another scatterer is by pair, which means that the rest of the scatterers are not present in this scattering process from one scatterer to another scatterer. Thus, one can use VSW for a scatterer and VPW for the dielectric substrate.
4. The final exciting fields are the unknowns in the Foldy–Lax multiple scattering equations. The final exciting field is valid around the scatterer, including the region inside the scatterer. There is no exclusion region for the exciting field.
5. There is no spatial discretization in the Foldy–Lax equations. Spatial discretizations cause a huge number of unknowns.
6. Since N is large, we use the FFT to have a fast summation of scattering from a large number of other scatterers.
7. After the final exciting field of scatterers is computed, we can calculate the fields “everywhere” by using the “single scatterer solution” of each scatterer.
8. For scatterers that are close to each other, just as the nearest neighbors, we can decompose them into near scatterers and non-near scatterers. Near-field wave interactions correspond to a sparse matrix⁴⁵.
9. Equation (1) is the Foldy–Lax equations in terms of exciting fields. We can also use the Foldy–Lax equation in terms of the scattered field.

$$E_q^s = T_q E^{inc} + T_q \sum_{p=1, p \neq q}^N G_{qp} E_p^s + T_q G_{q,sur} E_{sur}^s \quad (3)$$

$$E_{sur}^s = T_{sur} E^{inc} + T_{sur} \sum_{p=1}^N G_{sur,p} E_p^s \quad (4)$$

The scattered field formulations above are those of scattered waves to other scatterers. The scattered field formulation is to facilitate the computation of the final exciting field of a scatterer.

T matrix of a planar surface above a layered medium

Consider an incident wave upon the surface of the dielectric substrate. The incident exciting field \bar{E}^E of surface is in VPW,

$$\bar{E}^E = \int_{-\infty}^{\infty} dk_x \int_{-\infty}^{\infty} dk_y \exp(i\bar{K} \cdot \bar{r}) \left(a^{E(e)}(k_x, k_y) \hat{e}(k_x, k_y, -k_z) + a^{E(h)}(k_x, k_y) \hat{h}(k_x, k_y, -k_z) \right) \quad (5)$$

where (e) is TE polarization and (h) is TM polarization, $a^{E(e)}(k_x, k_y)$ and $a^{E(h)}(k_x, k_y)$ are respectively the exciting field coefficients for TE and TM respectively. The notations follow that of ref. 46, There are 4 T matrix components $T^{(ee)}(k_x, k_y, k'_x, k'_y)$, $T^{(eh)}(k_x, k_y, k'_x, k'_y)$, $T^{(he)}(k_x, k_y, k'_x, k'_y)$, $T^{(hh)}(k_x, k_y, k'_x, k'_y)$, where (k_x, k_y) and (k'_x, k'_y) are wave vector

components of the scattered wave and incident field, respectively. For plane waves with incident angle (θ_i, ϕ_i) and scattered angles (θ_s, ϕ_s) , the relations to wave vector components are $k_x = k \sin \theta_s \cos \phi_s, k_y = k \sin \theta_s \sin \phi_s, k'_x = k \sin \theta_i \cos \phi_i, k'_y = k \sin \theta_i \sin \phi_i$. In terms of T matrix coefficients

$$a^{s(e)}(k_x, k_y) = \int_{-\infty}^{\infty} \int_{-\infty}^{\infty} dk'_x dk'_y \left[T^{(ee)}(k_x, k_y, k'_x, k'_y) a^{E(e)}(k'_x, k'_y) + T^{(eh)}(k_x, k_y, k'_x, k'_y) a^{E(h)}(k'_x, k'_y) \right] \quad (6)$$

$$a^{s(h)}(k_x, k_y) = \int_{-\infty}^{\infty} \int_{-\infty}^{\infty} dk'_x dk'_y \left[T^{(he)}(k_x, k_y, k'_x, k'_y) a^{E(e)}(k'_x, k'_y) + T^{(hh)}(k_x, k_y, k'_x, k'_y) a^{E(h)}(k'_x, k'_y) \right] \quad (7)$$

The representation is a general expression of the surface and has been applied to a rough surface. In general, the T matrix coefficients can be computed by CEM, such as FEM, FD, or MoM, so that the T matrix coefficients are exact without approximations.

For the case of a planar surface with a layered medium, the T matrix can be obtained from the VPW of the scattered waves³⁴

$$\vec{E}^s = \int_{-\infty}^{\infty} dk_x \int_{-\infty}^{\infty} dk_y \exp(i\vec{k} \cdot \vec{r}) \left(R^{TE}(k_x, k_y) a^{E(e)}(k_x, k_y) \hat{e}(k_x, k_y, k_z) + R^{TM}(k_x, k_y) a^{E(h)}(k_x, k_y) \hat{h}(k_x, k_y, k_z) \right) \quad (8)$$

where $R^{TE}(k_x, k_y)$ and $R^{TM}(k_x, k_y)$ are TE and TM reflection coefficients of a layered medium. In the above formulations, the plane wave spectrum is $\int_{-\infty}^{\infty} dk_x \int_{-\infty}^{\infty} dk_y$, so that evanescent waves are included. For a discrete scatterer, the T matrix is in VSW³⁴ in this paper. For VSW, the exciting field is

$$\vec{E}^E = \sum_{m,n} \left(a_{mn}^{E(M)} Rg \bar{M}_{mn}(k\vec{r}) + a_{mn}^{E(N)} Rg \bar{N}_{mn}(k\vec{r}) \right) \quad (9)$$

The scattered field is

$$\vec{E}^S = \sum_{m,n} \left(a_{m,n}^{S(M)} \bar{M}_{mn}(k\vec{r}) + a_{m,n}^{S(N)} \bar{N}_{mn}(k\vec{r}) \right) \quad (10)$$

The T matrix in VSW is then defined by

$$a_{mn}^{S(M)} = \sum_{m',n'} \left(T_{mm'n'}^{(MM)} a_{m'n'}^{E(M)} + T_{mm'n'}^{(MN)} a_{m'n'}^{E(N)} \right) \quad (11)$$

$$a_{mn}^{S(N)} = \sum_{m',n'} \left(T_{mm'n'}^{(NM)} a_{m'n'}^{E(M)} + T_{mm'n'}^{(NN)} a_{m'n'}^{E(N)} \right) \quad (12)$$

where $n = 1, 2, \dots$ and $m = 0, \pm 1, \pm 2, \dots$. In notations, we can combine the two indices into 1, $(m, n) \rightarrow l$. VSW does not have evanescent wave components. Higher-order Vector Spherical waves have significant near fields, which are included in the VSW formulations.

Data availability

Data are available from the corresponding authors upon reasonable request.

Code availability

The underlying code for this study is not publicly available but may be made available to qualified researchers on reasonable request from the corresponding author.

Received: 6 June 2025; Accepted: 22 July 2025;

Published online: 07 November 2025

References

1. Kuznetsov, A. I. et al. Roadmap for optical metasurfaces. *ACS Photonics* **11**, 816–865 (2024).
2. Su, V.-C., Chu, C. H., Sun, G. & Tsai, D. P. Advances in optical metasurfaces: fabrication and applications. *Opt. Express* **26**, 13148 (2018).
3. Brongersma, M. L. et al. The second optical metasurface revolution: moving from science to technology. *Nat. Rev. Electr. Eng.* **2**, 125–143 (2025).
4. Quevedo-Teruel, O. et al. Roadmap for optical metasurface. *J. Opt.* **21**, 073002 (2019).
5. Wu, G. B. et al. 3-D-printed terahertz metalenses for next-generation communication and imaging applications. *Proc. IEEE* **PP**, 1–18 (2024).
6. Chen, J., Huang, S.-X., Chan, K. F., Wu, G.-B. & Chan, C. H. 3D-printed aberration-free terahertz metalens for ultra-broadband achromatic super-resolution wide-angle imaging with high numerical aperture. *Nat. Commun.* **16**, 363 (2025).
7. Solntsev, A. S., Agarwal, G. S. & Kivshar, Y. S. Metasurfaces for quantum photonics. *Nat. Photonics* **15**, 327–336 (2021).
8. Jha, P. K. et al. Metasurface-mediated quantum entanglement. *ACS Photonics* **5**, 971–976 (2018).
9. Chen, M. K., Liu, X., Sun, Y. & Tsai, D. P. Artificial intelligence in meta-optics. *Chem. Rev.* **122**, 15356–15413 (2022).
10. Bukhari, S. S., Whittow, W. G., Vardaxoglou, J. C. & Maci, S. Equivalent circuit model for coupled complementary metasurfaces. *IEEE Trans. Antennas Propag.* **66**, 5308–5317 (2018).
11. Jiang, Y., Dou, Y. & Gao, R. X. K. PEEC model based on a novel quasi-static Green's function for two-dimensional periodic structures. *IEEE J. Multiscale Multiphys. Comput. Tech.* **8**, 187–194 (2023).
12. Jin, J.-M. *Theory and Computation of Electromagnetic Fields* (John Wiley & Sons, Hoboken, NJ, 2015).
13. Taflove, A., Hagness, S. C. & Piket-May, M. Computational electromagnetics: the finite-difference time-domain method. *Electr. Eng. Handb.* **3**, 15 (2005).
14. Rumpf, R. C. *Electromagnetic and Photonic Simulation for the Beginner: Finite-Difference Frequency-Domain in MATLAB®* (Artech House, Hoboken, NJ, 2022).
15. Chew, W. C., Michielssen, E., Song, J. M. & Jin, J.-M. *Fast and Efficient Algorithms in Computational Electromagnetics* (Artech House, Inc., Norwood, MA, 2001).
16. Cai, G. et al. A full-vectorial spectral element method with generalized sheet transition conditions for high-efficiency metasurface/metafilm simulation. *IEEE Trans. Antennas Propag.* **71**, 2652–2660 (2023).
17. Crocco, L., Cuomo, F. & Isernia, T. Generalized scattering-matrix method for the analysis of two-dimensional photonic bandgap devices. *J. Opt. Soc. Am. A.* **24**, A12–A22 (2007).
18. Patel, U. R., Triverio, P. & Hum, S. V. A fast macromodeling approach to efficiently simulate inhomogeneous electromagnetic surfaces. *IEEE Trans. Antennas Propag.* **68**, 7480–7493 (2020).
19. Jiang, M. et al. Efficient and accurate simulations of metamaterials based on domain decomposition and unit feature database. *IEEE Trans. Antennas Propag.* **72**, 8635–8646 (2024).
20. Li, J. et al. Addressable metasurfaces for dynamic holography and optical information encryption. *Sci. Adv.* **4**, eaar6768 (2018).
21. Zhou, Y. et al. Analog optical spatial differentiators based on dielectric metasurfaces. *Adv. Opt. Mater.* **8**, 1901523 (2020).

22. Ueno, A., Hu, J. & An, S. Ai for optical metasurface. *npj Nanophotonics* **1**, 36 (2024).
23. Zhou, W. et al. An inverse design paradigm of multi-functional elastic metasurface via data-driven machine learning. *Mater. Des.* **226**, 111560 (2023).
24. Jiang, J. & Fan, J. A. Global optimization of dielectric metasurfaces using a physics-driven neural network. *Nano Lett.* **19**, 5366–5372 (2019).
25. Ji, W. et al. Recent advances in metasurface design and quantum optics applications with machine learning, physics-informed neural networks, and topology optimization methods. *Light Sci. Appl.* **12**, 169 (2023).
26. Jeong, J., Tsang, L., Gu, W., Colliander, A. & Yueh, S. H. Wave propagation in vegetation field by combining fast multiple scattering theory and numerical electromagnetics in a hybrid method. *IEEE Trans. Antennas Propag.* **71**, 3598–3610 (2023).
27. Jeong, J. et al. Full-wave simulations of forest at L-band with fast hybrid multiple scattering theory method and comparison with GNSS signals. *IEEE J. Sel. Top. Appl. Earth Obs. Remote Sens.* **18**, 5395–5405 (2025).
28. Jeong, J. *Fast Hybrid Multiple Scattering Theory Method Applied to Multiple Scattering Problems*. Ph.D. thesis, University of Michigan (2025).
29. Yang, J., Zhou, H. & Lan, T. All-dielectric reflective metasurface for orbital angular momentum beam generation. *Opt. Mater. Express* **9**, 3594 (2019).
30. Lian, Y. et al. OAM beam generation in space and its applications: a review. *Opt. Lasers Eng.* **151**, 106923 (2022).
31. Matiushchikina, M. et al. Design and experimental demonstration of wavelength-selective metamirrors on sapphire substrates. *Adv. Photonics Res.* **2400116**, 1–10 (2024).
32. Zhang, K., Wang, Y., Yuan, Y. & Burokur, S. N. A Review of orbital angular momentum vortex beams generation: from traditional methods to metasurfaces. *Appl. Sci.* **10**, 1015 (2020).
33. Gao, R. et al. Fast calculations of band diagrams of irregularly shaped scatterers in periodic structures using the multiple scattering theory and broadband Green's function. *Opt. Express* **32**, 43553–43570 (2024).
34. Liao, T.-H., Gao, R., Huang, Z., Tsang, L. & Tan, S. Fast calculations of band diagrams of photonic crystals with dense scatterers using t-matrix extractions and multiple scattering theory with broadband Green's functions. *Opt. Express* **33**, 27079–27097 (2025).
35. Tsang, L., Chen, H., Huang, C.-C. & Jandhyala, V. Modeling of multiple scattering among vias in planar waveguides using Foldy–Lax equations. *Microw. Opt. Technol. Lett.* **31**, 201–208 (2001).
36. Fujii, H. et al. Photon transport model for dense polydisperse colloidal suspensions using the radiative transfer equation combined with the dependent scattering theory. *Opt. Express* **28**, 22962–22977 (2020).
37. Hofgartner, J. D. & Hand, K. P. A continuum of icy satellites' radar properties explained by the coherent backscatter effect. *Nat. Astron.* **7**, 534–540 (2023).
38. Safadi, M. et al. Coherent backscattering of entangled photon pairs. *Nat. Phys.* **19**, 562–568 (2023).
39. Bai, X., Li, R., Tan, S., Mikki, S. & Li, E. An electromagnetic analysis of the impact of random scattering and RISs on the Shannon capacity of MIMO communication systems. *IEEE Antennas Wirel. Propag. Lett.* **23**, 1176–1180 (2023).
40. Foldy, L. L. The multiple scattering of waves. I. General theory of isotropic scattering by randomly distributed scatterers. *Phys. Rev.* **67**, 107 (1945).
41. Lax, M. Multiple scattering of waves. *Rev. Mod. Phys.* **23**, 287 (1951).
42. Enrica Martini, S. M. & Giacomo, Carli A domain decomposition method based on a generalized scattering matrix formalism and a complex source expansion. *Prog. Electromagn. Res. B.* **19**, 445–473 (2010).
43. Tsang, L., Kong, J. A. & Shin, R. T. *Theory of microwave remote sensing* (Wiley, New York, NJ USA, 1985).
44. Tsang, L., Chen, H., Huang, C. C. & Jandhyala, V. Modeling of multiple scattering among vias in planar waveguides using Foldy–Lax equations. *Microw. Opt. Technol. Lett.* **31**, 201–208 (2001).
45. Tsang, L., Kong, J. A., Ding, K.-H. & Ao, C. O. *Scattering of Electromagnetic Waves: Numerical Simulations* (John Wiley & Sons, New York, NY, 2001).
46. Tsang, L., Kong, J. A. & Ding, K.-H. *Scattering of Electromagnetic Waves: Theories and Applications* Vol. 15 (John Wiley & Sons, New York, NY, 2000).

Acknowledgements

This work is supported by the University of Michigan. The authors thank Altair Engineering for granting the full version of FEKO to the University of Michigan. The authors have filed a provisional patent application related to the major subject matter of this manuscript. [Applicant(s): The Regents of The University of Michigan, Ann Arbor, MI. Inventor(s): Leung TSANG, Ann Arbor, MI; Jongwoo JEONG, Ann Arbor, MI; Zhengming HUANG, Ann Arbor, MI. Provisional Application No. 63/772,006, filed on 03/25/2025]. It covers the major content of this paper. Note: In the patent, "Zhengming Huang" is a misspelling of the author's name, which should be "Zhenming Huang," as in this paper. It will be corrected in the future.

Author contributions

L.T. conceived the research, proposed the theory, developed the equations, wrote some the code, and wrote part of the paper. Z.H. wrote the complete code, performed the numerical experiments, obtained the simulation results, and wrote the paper. J.J. contributed data and tools. All authors read and approved the final manuscript.

Competing interests

The authors declare no competing interests.

Additional information

Supplementary information The online version contains supplementary material available at <https://doi.org/10.1038/s44455-025-00006-5>

Correspondence and requests for materials should be addressed to Leung Tsang.

Reprints and permissions information is available at <http://www.nature.com/reprints>

Publisher's note Springer Nature remains neutral with regard to jurisdictional claims in published maps and institutional affiliations.

Open Access This article is licensed under a Creative Commons Attribution-NonCommercial-NoDerivatives 4.0 International License, which permits any non-commercial use, sharing, distribution and reproduction in any medium or format, as long as you give appropriate credit to the original author(s) and the source, provide a link to the Creative Commons licence, and indicate if you modified the licensed material. You do not have permission under this licence to share adapted material derived from this article or parts of it. The images or other third party material in this article are included in the article's Creative Commons licence, unless indicated otherwise in a credit line to the material. If material is not included in the article's Creative Commons licence and your intended use is not permitted by statutory regulation or exceeds the permitted use, you will need to obtain permission directly from the copyright holder. To view a copy of this licence, visit <http://creativecommons.org/licenses/by-nc-nd/4.0/>.

© The Author(s) 2025